JMEPEG (2017) 26:1589–1597
DOI: 10.1007/s11665-017-2568-z

1059-9495/$19.00

Microstructure Characterization and Corrosion Resistance Behavior of New Cobalt-Free Maraging Steel Produced Through ESR Techniques

Asiful H. Seikh, Hossam Halfa, Muneer Baig, and Sohail M.A. Khan

(Submitted April 12, 2016; in revised form January 2, 2017; published online March 13, 2017)

In this study, two different grades (M23 and M29) of cobalt-free low nickel maraging steel have been produced through electroslag remelting (ESR) process. The corrosion resistance of these ESR steels was investigated in 1 M H_2SO_4 solution using linear potentiodynamic polarization (LPP) and electrochemical impedance spectroscopy (EIS) techniques. The experiments were performed for different immersion time and solution temperature. To evaluate the corrosion resistance of the ESR steels, some significant characterization parameters from LPP and EIS curves were analyzed and compared with that of conventional C250 maraging steel. Irrespective of measurement techniques used, the results show that the corrosion resistance of the ESR steels was higher than the C250 steel. The microstructure of ESR steels was composed of uniform and well-distributed martensite accompanied with little amount of retained austenite in comparison with C250 steel.

Keywords corrosion resistance, electrochemical impedance spectroscopy, maraging steels, microstructure, polarization

1. Introduction

During the last few decades, ultra-high strength maraging steels have been used in a wide applications including missile and rocket motor cases, aircraft, aerospace nuclear and gas turbine applications (Ref 1-4). In general, maraging steels are usually low-carbon nickel-based alloys with substantial amount of Co, Mo along with small percentages of Ti and Al. However, depending on the application, the composition of the material can be modified (Ref 5, 6). Due to the low carbon content, maraging steels generally possess high machinability (Ref 7). Addition of chromium leads to the production of corrosion-resistant grades (Ref 8). The maraging steels have high strength, good weldability and superior fracture toughness than the conventional steels (Ref 9). The maraging steels exhibit good dimensional stability at high temperatures due to their high thermal conductivity. The characteristic ultra-high strength of maraging steels is mostly attributed to the precipitation of intermetallic compounds during the aging process (Ref 10-12). High nickel maraging steels are very sensitive to two phenomena, namely austenitic reversion phenomenon and over-aging problem that deteriorate their mechanical properties. Vanderwalker (Ref 13) observed that the finest particle of Ni_3Ti nucleates more easily and faster than the Ni_3Mo particles. This observation is very valuable because, new grades of maraging steels can be produced by partial or complete substitution of Mo with Ti. This substitution would not only reduce the cost of maraging steels but negate the problem of over-aging as well. It is known that the primary strengthening effect in conventional maraging steel is mainly due to the presence of nickel and molybdenum. Cobalt is used to increase the transformation temperature and to facilitate the formation of molybdenum intermetallic precipitation (Ni_3Mo, Fe_2Mo and Fe_7Mo_6). Thus, the presence of cobalt in maraging steels is highly desirable, but its presence results in substantial increase in the manufacturing costs. To reduce the manufacturing costs, it is desired to produce cobalt-free maraging steels by replacement with Ti as the primary strengthening element. The addition of titanium to such steels promotes the precipitation of Ni_3Ti intermetallic compound instead of Fe_2Mo or Fe_7Mo_6. Furthermore, to overcome the problem of retained austenite, it is suggested that the nickel content be reduced to 12% or less (Ref 14, 15).

The electroslag remelting (ESR) process has been successfully used to remelt maraging steel instead of the double-vacuum technique which is recommended by Bohler Edelstahl GmbH & Co. The improvement in the quality of refined steels produced by ESR process arises from the production of sound ingots with the complete absence of pipes and porosity, clean smooth surface and high product yield. The structure of ESR ingots is improved through the uniformity, elimination of banding and zone segregation and control of grain size (Ref 11-13). By using ESR technique, the reduction in segregation, grain size and nonmetallic inclusions (NMI) will be reflected positively on the corrosion and mechanical properties of the developed steels (Ref 15).

The maraging steels when exposed to several acids during pickling, descaling and acidizing processes lead to the formation of scales and corrosion on its surface. The currently available literature presents a brief report on the corrosion behavior of 18 Ni maraging steel which is reportedly in

Asiful H. Seikh and **Muneer Baig**, Centre of Excellence for Research in Engineering Materials, Advanced Manufacturing Institute, King Saud University, P.O. Box - 800, Riyadh 11421, Saudi Arabia; **Hossam Halfa**, Steel Technology Department, Central Metallurgical R&D Institute (CMRDI), Helwan, Egypt; and **Sohail M.A. Khan**, Mechanical Engineering Department, College of Engineering, King Saud University, P.O. Box - 800, Riyadh 11421, Saudi Arabia. Contact e-mail: aseikh@ksu.edu.sa.

martensite phase and the atmospheric exposure of 18 Ni maraging steel leads to uniform corrosion. Bellanger and Rameau (Ref 16) have studied the effect of slightly acidic pH with or without chloride ions in radioactive water on the corrosion resistance of maraging steel. They have reported that the corrosion behavior of maraging steel depends on pH of the solution and the intermediates formed on the maraging steel surface in the active region. The effect of carbonate ions in a slightly alkaline medium on the corrosion of maraging steel was studied by Bellanger (Ref 17). It is known that the diffusion of hydrogen in maraging steels is pretty low. This is due to the fact that maraging steels are less liable to hydrogen embrittlement when compared to low-carbon steel (Ref 18). The investigation of corrosion behavior of aged and annealed 18 Ni 250 grade maraging steel in a phosphoric and sulfuric acid medium revealed that the corrosion rate of the annealed sample is less than the corrosion rate of the aged sample (Ref 4, 19).

In this work, two new grades of cobalt-free maraging steels (M23 and M29) were developed using ESR process. The corrosion behavior of the developed steels was further investigated and compared against the response of conventional C250 maraging steel in 1 M H_2SO_4 solution using LPP and EIS techniques.

2. Experimental

2.1 Materials Preparation

In this work, two different grades of maraging steels (cobalt-free, low nickel) produced by ESR technique process was studied. The detailed description on the method and processing conditions was published elsewhere (Ref 14, 15). Table 1 shows the chemical composition of investigated steels.

Initially, the two grades (M-23 and M-29) of cobalt-free maraging steel and conventional C-250 maraging steel were cut into small pieces with dimension 1 × 1 × 0.5 cm from the delivered sheets. Two pieces of each grade were used as the test material.

2.2 Phase Identification

One of the surfaces of the test specimens of each grade were mechanically polished with silicon carbide abrasive papers ranging from 60 to 1000 grit followed by cloth polishing using colloidal silica solution to produce a scratch-free mirror surface. The polished specimens were later cleaned and washed with alcohol and air-dried. The etching of the specimens was done using 2% nital solution (2% HNO_3 in methanol). The microstructure of the etched samples was investigated using an optical microscope. Alternatively, x-ray diffraction (XRD) was used to determine quantitatively the phases present in the processed material.

The XRD was performed on the heat treated steel in a diffractometer using Cu-k_α radiation for quantitative determination of retained austenite. The percentage of retained austenite formed during the aging treatment was determined by the direct comparison of the integrated intensities of (110) and (200) planes of the martensite phase with the intensities of (111) and (200) planes of the austenite phase (Ref 20).

2.3 Experimental Procedure

The electrochemical experiments were performed in a three-electrode cell system where the developed maraging steel specimens were used as the working electrode (WE), a platinum foil as the counter electrode (CE) and Ag/AgCl as the reference electrode. The solution used was 1 M H_2SO_4 solution, prepared from analytical grade reagents and distilled water. To prepare the WE, one of the surfaces of the steel specimens was connected to a copper wire by soldering technique. The soldered specimen was then mounted in an epoxy resin with hardener. After curing, the free surface of the sample was polished with silicon carbide abrasive papers ranging from 60 to 1000 grit followed by cloth polishing.

The linear potentiodynamic polarization (LPP) and electrochemical impedance spectroscopy (EIS) experiments were performed using an Autolab system. The EIS tests were performed after immersing the steel specimens in the test solution for 10 min, 60 min, 120 min and 24 h at open-circuit potential (EOC) to confirm its stability with time. The EIS were measured with electrochemical cell at EOC with an applied 5 mV sinusoidal perturbations in the frequency range of 100 kHz ~ 100 mHz with 10 steps per decade. The LPP was conducted from the EOC at the same positions and immediately after the EIS measurements. These tests were conducted by stepping the potential at a scan rate of 1 mV s^{-1} in the range of −1000 to +100 mV against SCE at OCP. Each test was performed at least three times to obtain statistically significant results.

3. Results and Discussion

3.1 Microstructural Characterization

The microstructure of ESR steels and standard C250 (18 Ni 250) steel after full heat treatment (optimum solid solution annealing and aging conditions) was composed of martensite and retained austenite. Figure 1 shows that the microstructure of ESR steels is very fine and free from segregation or band structure, while the microstructure of C250 steel showed lamellar morphology with unresolved bright patchy area (retained austenite-black arrows). The quantity of retained austenite for the developed steels was measured by XRD using comparison method, as shown in Fig. 2.

Figure 1(a) shows the optical micrographs of the C250 steel produced by vacuum arc remelting and aged under optimum

Table 1 Chemical composition of C-250, M-23 and M-29 maraging steel

	C	Cr	Co	Mo	Ni	Ti	W	Al	Fe
C-250	0.03	…	7.5	4.8	18	0.4	…	0.4	Balance
M-23	0.0325	0.004	…	1.76	11.16	0.641	1.11	0.102	Balance
M-29	0.077	0.0153	…	1.62	10.67	0.511	1.01	0.059	Balance

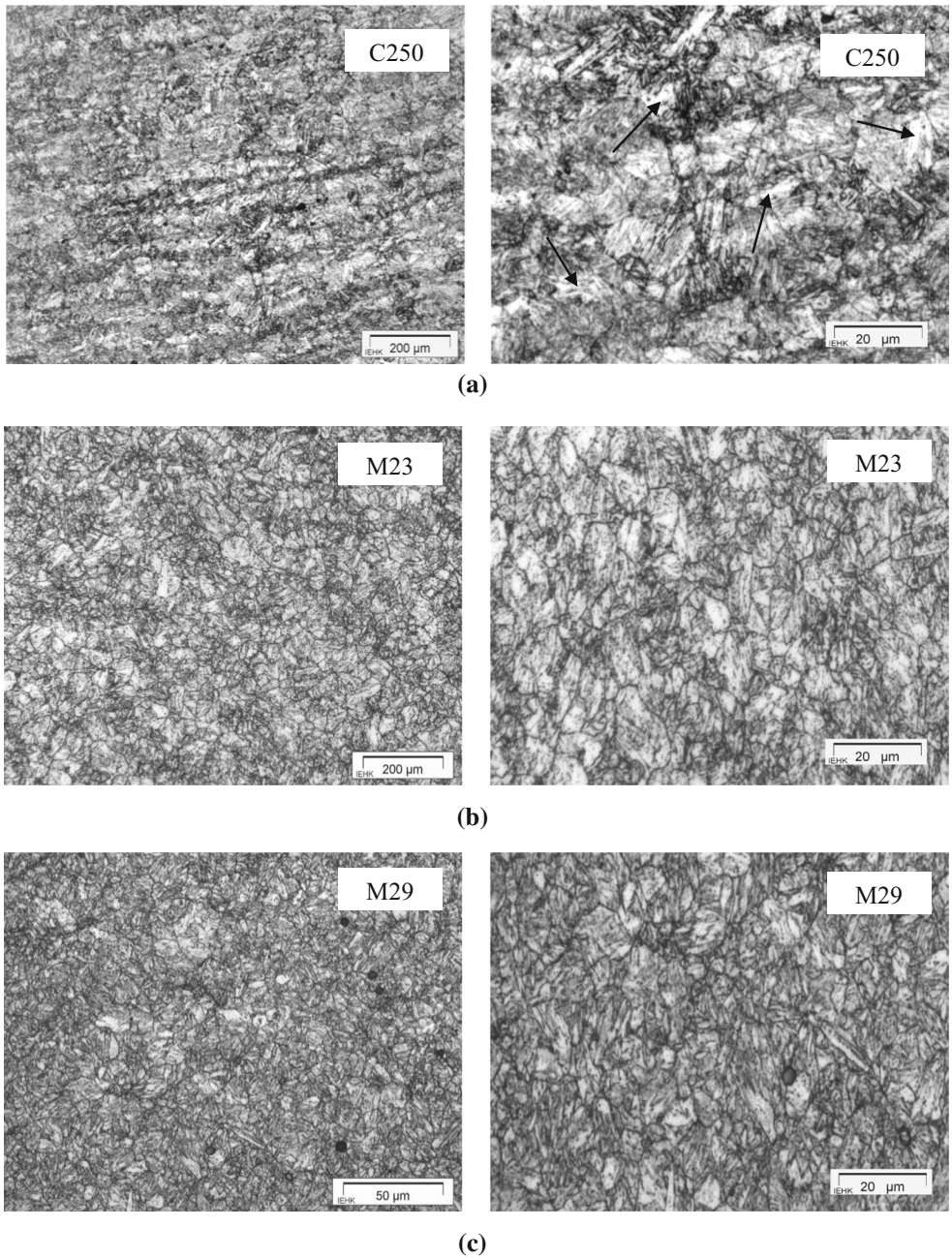

Fig. 1 Microstructure of investigated steels [C250 (a), M23 (b) and M29 (c)] in full heat treatment condition

condition. The microstructure consisted of lamellar morphology with unresolved bright patchy areas. These areas represent regions that possess substantial volume fraction of reverted austenite and the prior-austenite grain boundaries could not be resolved easily. The existence of inter-lath austenite, though not fully resolved, is also shown in the microstructure. On the other hand, microstructure of the ESR steels (M23 and M29) after full heat treatment at optimum conditions showed packets of martensite, within prior-austenite grains. In case of ESR steels, Fig. 1(b), (c) shows that the martensite packet could be recognized not only due to the preferential etching along their boundaries but also due to martensite packets within an austenite grain that did not extend beyond the respective prior-austenite grain boundary.

The amount of retained austenite that formed C250 and ESR steels were studied using x-ray diffraction (XRD) technique. The XRD results showed the presence of about $10 \pm 0.5\%$ retained austenite in C250 steels after solid solution annealing treatment, while the ESR steels after full heat treatment contained about $1 \pm 0.5\%$ retained austenite. Based on the experimental results obtained from XRD it is observed that, the solution-treatment has resulted in the complete martensite transformation in ESR steels. Table 2 shows the austenite contents for various steels as detected by XRD analysis.

It well known that the maraging steel is a high-strength precipitation steel which get full strength after aging through precipitation hardening reactions at optimum condition. It was reported in several investigations (Ref 15, 20, 21) that Ni_3Mo,

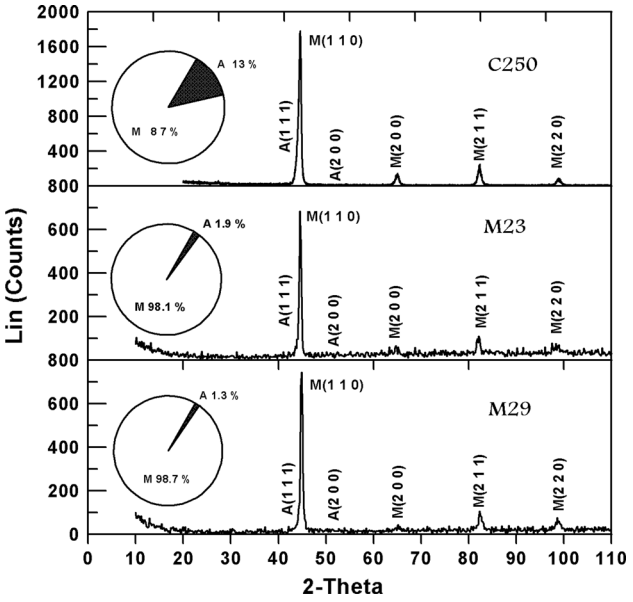

Fig. 2 X-ray pattern of investigated steel after full heat treatment (optimuim solid solution and aging conditions)

Table 2 Retained austenite measurements by x-ray for investigated steel

Steel No.	Process	Net austenite, % by x-ray	
		Annealed	Aged
C250	Vacuum	10	13
M23	ESR3	1.5	1.9
M29	ESR1	1.1	1.3

Fe_2Mo or the σ phase intermetallic compound was precipitated for cobalt-free molybdenum containing maraging steel. For cobalt-free maraging steel containing molybdenum at optimum aging condition (480 °C), the precipitation occurs as Ni_3Mo while over-aging process leads to the replacement of Ni_3Mo by either Fe_2Mo or the σ phase. For maraging steel containing titanium, it was reported that the titanium may totally or partially replace the molybdenum in precipitated intermetallic compound, i.e., as Ni_3Ti or Ni_3(Mo, Ti) (Ref 22).

It is clear from Table 2 and Fig. 2 that the amount of retained austenite in the ESR steels does not depend entirely on the chemical composition of the investigated steels but also on its production condition. Increasing the amount of alloying elements, i.e., Co, Mo, Cr and Ti is accompanied by increasing the tendency to form retained austenite. ESR has advantages that it has low local solidification time (LST) than the conventional casting method. The cooling rates estimated using the Rosenthal theory (Ref 23, 24) is of the order of 100 °C s^{-1}, while the local cooling rate in vacuum ingots is 5-25 °C s^{-1}. This is an important difference of the ESR process compared to the vacuum melting technique that leads to a very fine and well-distributed microstructures compared to vacuum melting steels as shown in Fig. 1.

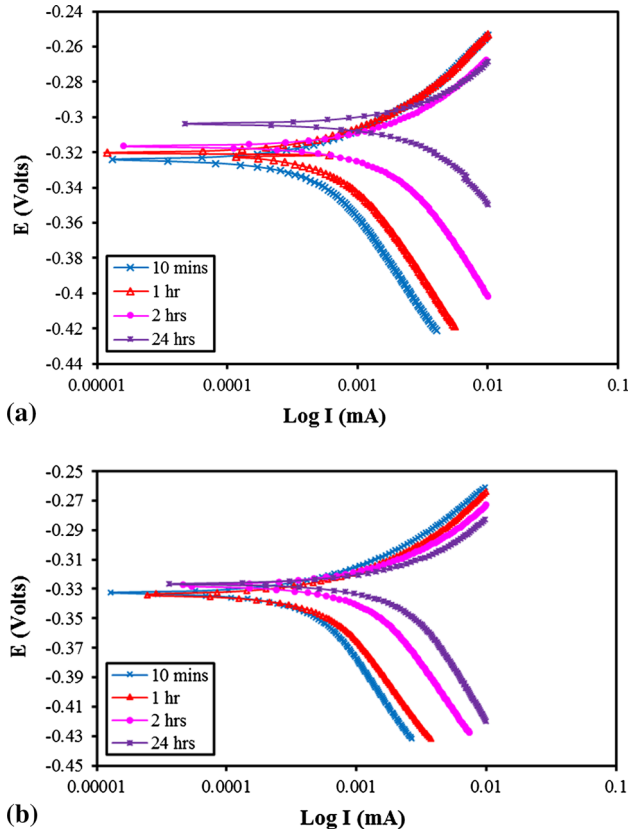

Fig. 3 Potentiodynamic polarization curves for M-23(a) and M-29(b) maraging steel samples in 1 M H2SO4 solutions at room temperature

3.2 Electrochemical Measurements

3.2.1 Effect of Immersion Time. The polarization curves for ESR steel specimens (M23 and M29) in 1 M H_2SO_4 solution after 10 min, 60 min, 120 min and 24 h of immersion at room temperature are shown in Fig. 3(a), (b). The values of corrosion potential (E_{corr}), corrosion current density (J_{corr}) and polarization resistance (R_p) that were obtained from the LPP curves are listed in Table 3. From polarization curve, it is evident that the cathodic current of the ESR steels move to less negative value with increasing the potential till the current reaches its minimum at the corrosion current density, J_{corr}.

The corrosion current density, J_{corr}, was determined graphically by extrapolating the cathodic and anodic Tafel slopes to the E_{corr} (versus Ag/AgCl). From the polarization diagram (Fig. 3) and Table 3, it is observed that with an increase in immersion time, values of anodic and cathodic currents J_{corr} increases and the values of E_{corr} shifted toward the more positive direction. It is also confirmed from Table 3 that with immersion time the polarization resistance (R_p) decreases. Thus, it can be concluded that with an increase in immersion time, the dissolution or rate of corrosion in the maraging steels increases due to the aggressive action of sulfuric acid. The reaction mechanisms of the dissolution of iron in acid medium can be found elsewhere (Ref 25). However, due to the continuous attack of sulfuric acid onto the steel surface, the formation of oxides/or corrosion products is hampered. Further increasing the applied potential in the positive direction allow

Table 3 Potentiodynamic polarization parameters of maraging specimens in 1 MH_2SO_4 at room temperature after 10-min, 60-min, 120-min and 24-h immersions

Tafel data						LPP data
Materials	**Time**	**b_a mV/decade**	**b_c mV/decade**	**E_{corr} mV**	**J_{corr} µA**	**R_p Ω**
M23	10 min	37.31	24.41	−324	206.10	31.09
	60 min	26.08	22.69	−321	217.36	24.24
	120 min	32.46	26.26	−316	555.23	11.36
	24 h	20.26	22.91	−304	846.47	5.52
M29	10 min	37.86	21.87	−332	172.55	34.89
	60 min	34.59	20.09	−334	197.60	28.70
	120 min	39.24	26.33	−328	454.96	15.04
	24 h	41.02	26.62	−326	758.08	9.25

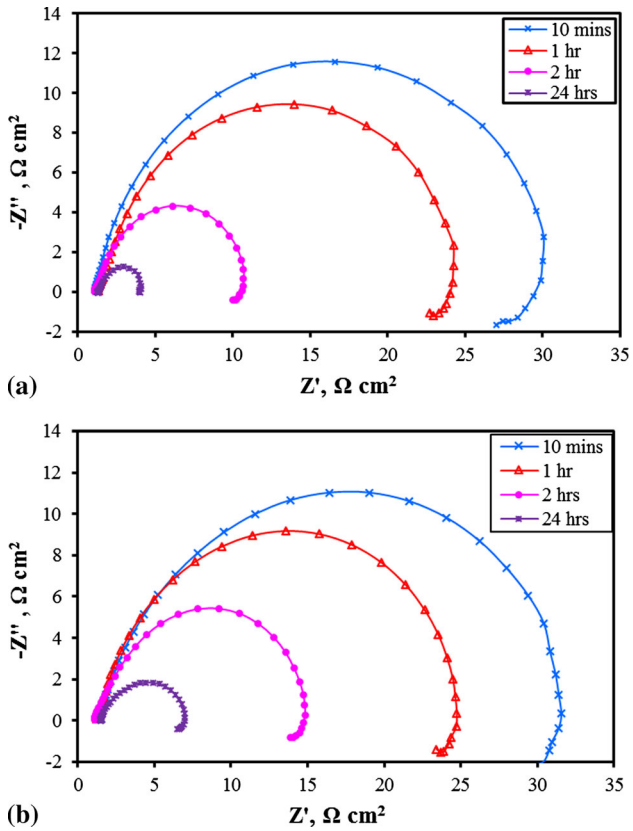

Fig. 4 EIS [Nyquist plot] for M-23(a) and M-29(b) maraging steel samples in 1 M H2SO4 solutions at room temperature

the steels to corrode more due to increase in anodic current as shown in the polarization curves (Fig. 3).

The corrosion response of ESR steel specimens in 1 M H_2SO_4 solution was studied using EIS technique in order to determine their mechanistic and kinetic parameters and to compare the results obtained from potentiodynamic polarization. Nyquist plot obtained at the open-circuit potential for M23 and M 29 grades at different exposure times are shown in Fig. 4(a), (b). The Nyquist plots were analyzed by fitting the experimental results to an equivalent circuit model shown in Fig. 5. The circuit consists of a parallel combination of a constant phase element (CPE, Q), the charge-transfer resistance (R_{ct}) corresponding to the corrosion reaction at metal/electrolyte interface and the solution resistance (R_s) between the

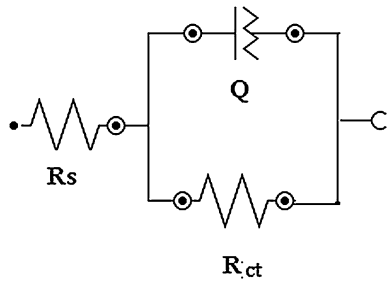

Fig. 5 Equivalent circuit fitting for EIS

working and reference electrode (Ref 26, 27). To reduce the effects due to surface irregularities of metal, constant phase element (CPE, Q) is introduced into the circuit instead of a pure double-layer capacitance (C_{dl}) which gives the more accurate fit (Ref 28). Among these parameters, R_{ct} is the factor that determines corrosion resistance of alloys. Since, R_{ct} is inversely proportional to J_{corr}, a higher value of R_{ct} corresponds to a lower value of J_{corr}. The impedance of CPE can be expressed as $Z_{CPE} = 1/Y_0\ (j\omega)^n$, where Y_0 is the CPE constant, n is the exponent (phase shift), ω is the angular frequency and j is the imaginary unit. CPE may be resistance, capacitance and inductance depending upon the values of n (Ref 25). In all experiments, the observed value of n ranges between 0.8 and 1.0, suggesting the capacitive response of CPE. From this circuit R_s, R_{ct} and C_{dl} were determined and are shown in Table 4.

The Nyquist plots for ESR steels consist of a depressed capacitive loop which could be related with the charge-transfer reaction from the alloy into the electrolyte through the electrochemical double layer. From the Nyquist plot, it is noted that the diameter of the loop/arc decreases with the increase in immersion time indicating that the double-layer capacitance (C_{dl}) increases and charge-transfer resistance (R_{ct}) decreases substantially with the increase in immersion time. The results from Table 4 confirm that the values of R_{ct} decrease with the immersion time. These observations indicate that the corrosion in steel is controlled by a charge-transfer process (Ref 29).

Bode plots shown in Fig. 6(a), (b) indicate the presence of one time constant, corresponding to the one depressed semicircle that obtained in case of Nyquist plots. The Bode plot was examined to observe the changes on the surface of the sample during EIS experiment. The decrease in impedance values of Bode plot implies that the corrosion resistance of the steels decreases with immersion time.

Table 4 Electrochemical impedance parameters of maraging specimens in 1 MH_2SO_4 at room temperature after 10-min, 60-min, 120-min and 24-h immersions

Materials	Time	R_s Ω	CPE mMho	n	R_{ct} Ω
M23	10 min	1	0.956	0.847	30
	60 min	1.5	1.69	0.845	23.8
	120 min	1.2	3.23	0.897	10
	24 h	1.4	28	0.92	2.8
M29	10 min	1.2	1.22	0.762	32.2
	60 min	1.2	1.41	0.817	24.5
	120 min	1.2	2.90	0.801	14.6
	24 h	1.65	5.49	0.728	7.5

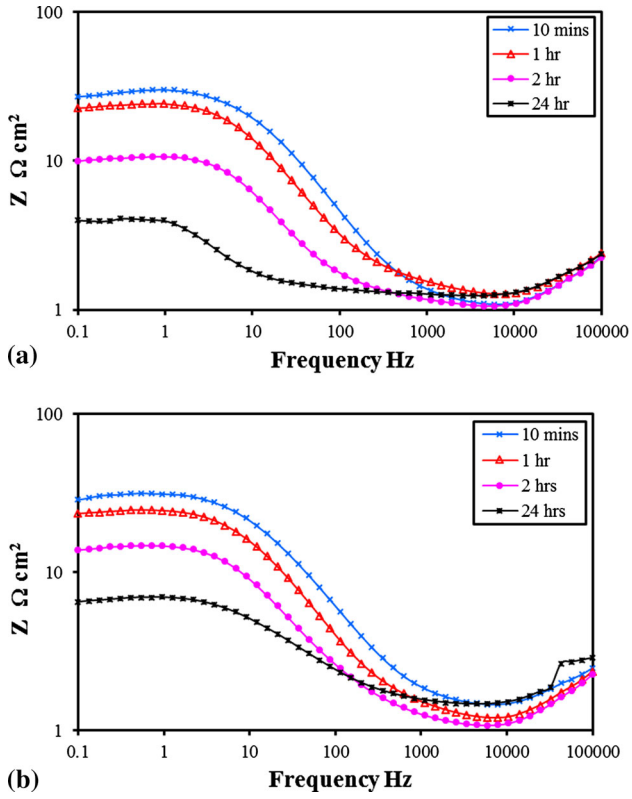

Fig. 6 Bode plot for M-23(a) and M-29(b) maraging steel samples in 1 M H2SO4 solutions at room temperature

3.2.2 Effect of Solution Temperature. The corrosion resistances of ESR steels in 1 M H_2SO_4 solution were carried out at higher temperatures. Figures 7 and 8 show the potentiodynamic polarization curves and Nyquist plots, respectively, at different temperatures between 20 and 50 °C. The parameters obtained from polarization curves and EIS plots are listed in Tables 5 and 6.

It has been seen from Fig. 7 and 8 that with an increase in temperature of solution, the corrosion resistance of the steels decreases. This observation may be due to the effect of temperature on the corrosion resistance of steel. With an increase in temperature, the hydrogen evolution over potential decreases and leads to the enhancement in the cathodic reaction rate (Ref 30). Changes in the cathodic and anodic slopes (β_c and β_a) of the polarization curves with the increase in

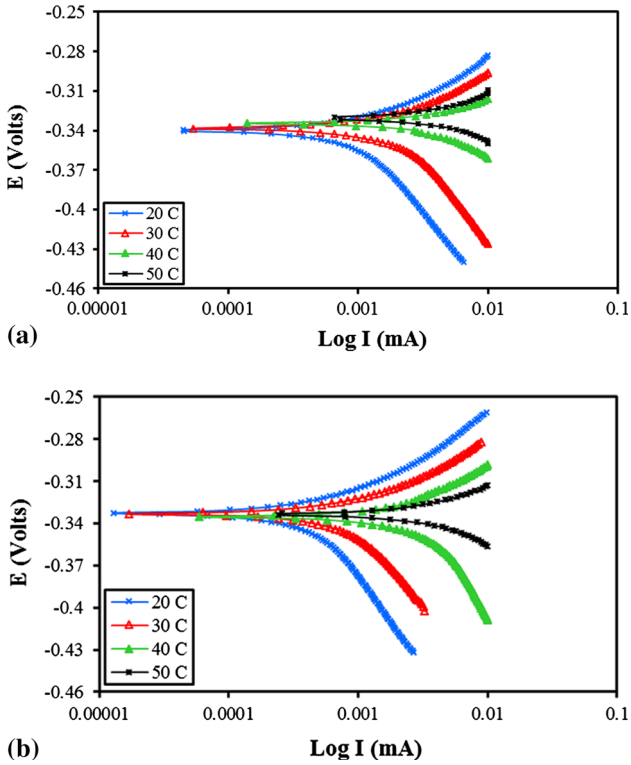

Fig. 7 Potentiodynamic polarization curves for M-23(a) and M-29(b) maraging steel samples in 1 M H2SO4 solutions at different temperature

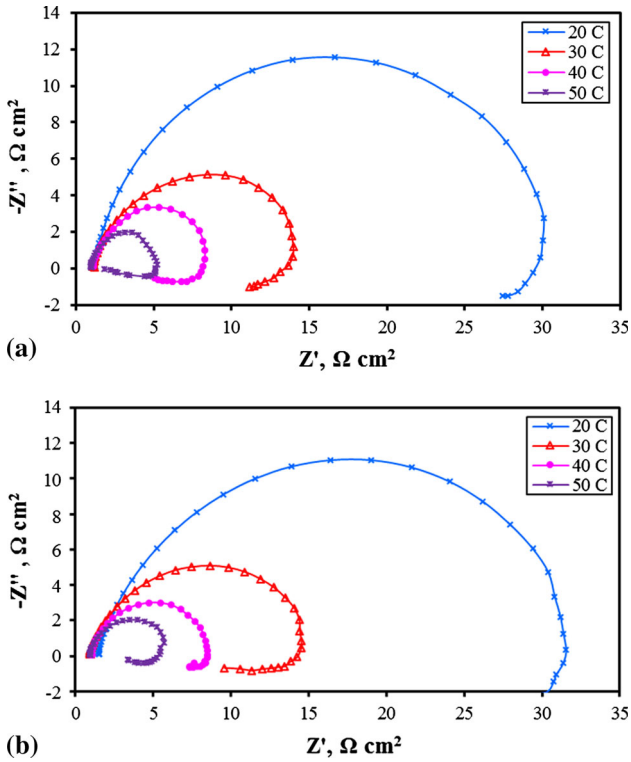

Fig. 8 EIS [Nyquist plot] for M-23(a) and M-29(b) maraging steel samples in 1 M H2SO4 solutions at different temperature

immersion time and temperature indicate that the acid concentration and solution temperature play an important role on the kinetics of hydrogen evolution and metal dissolution. The observed negative inductive loops in the fourth quadrant of Nyquist plots are associated with the dissolution of steel in acid solution with an increase in time and temperature.

3.3 Corrosion Resistance Comparison with Conventional Maraging Steel

The corrosion-resistant properties of the investigated ESR steels have been compared with the C250 steel. The polarization curves for ESR (M23 and M29) steels C250 steel in 1 M H_2SO_4 solution after 10 min of immersion at room temperature are shown in Fig. 9. The polarization parameters obtained from the curves are as shown in Table 7. Comparing the polarization curves of cobalt-free ESR steels with the conventional C250 steel, the polarization curve of C250 maraging steel shifted toward more anodic (positive) region and the J_{corr} values of C250 was higher than ESR steels as shown in Fig. 7. It is also seen that the corrosion resistance (R_p) of ESR steel is more than that of C250 grade. The percentage of retained austenite significantly influences the corrosion properties of C250 steel, limiting its usefulness as a high-strength material. Further deterioration in the corrosion properties of maraging steels is obtained by micro-segregation of retained austenite in localized area, i.e., the solute segregation to the existing areas that causes galvanic corrosion. It has been discussed previously (section 3.1) that amount of retained austenite for the investigated

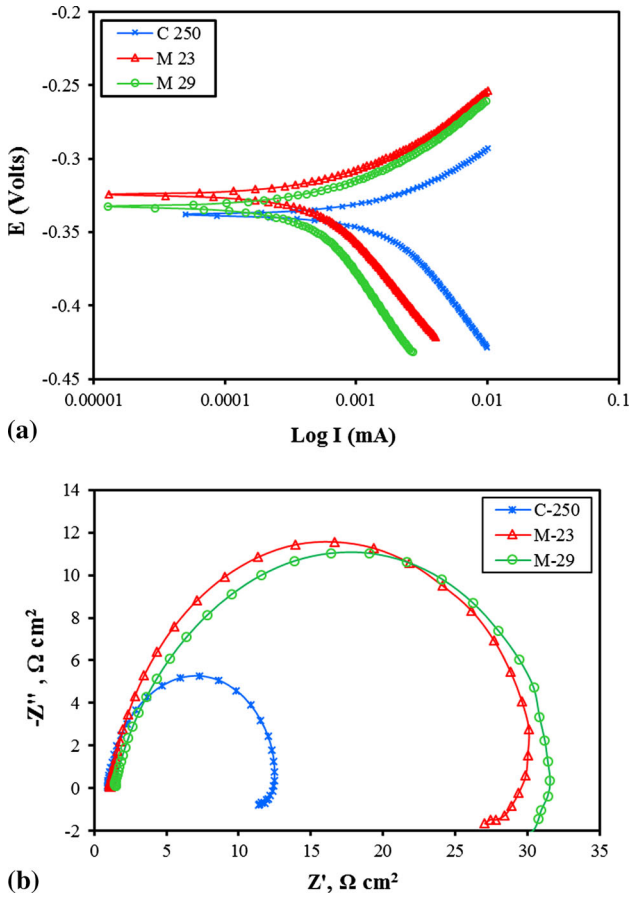

Fig. 9 Potentiodynamic polarization (a) and EIS [Nyquist plot] (b) for maraging steel samples after 10-min immersion in 1 M H2SO4

Table 6 Electrochemical impedance parameters of M-23 and M-29 maraging steel in 1M H_2SO_4 at different temperature

EIS data					
Materials	**Temperature, °C**	**R_s Ω**	**CPE mMho**	***n***	**R_{ct} Ω**
M-23	20	1	0.956	0.847	30
	30	1.2	1.06	0.854	12.8
	40	1.07	1.21	0.863	9.2
	50	0.86	1.48	0.837	4.45
M-29	20	1.2	1.02	0.762	32.2
	30	0.8	1.15	0.778	14.6
	40	0.94	1.22	0.858	8.7
	50	0.87	1.29	0.828	5.40

Table 7 Polarization parameters of maraging specimens in 1MH_2SO_4 at room temperature

Tafel data					LPP data
	b_a mV/decade	**b_c mV/decade**	**E_{corr} mV**	**J_{corr} µA**	**R_p Ω**
C-250	38.07	25.74	−338	620.35	10.75
M23	37.31	24.41	−324	206.10	31.09
M29	37.86	21.87	−332	172.55	34.89

Table 5 Potentiodynamic polarization parameters of M-23 and M-29 maraging steel in 1M H_2SO_4 at different temperature

Tafel data						LPP data
Materials	**Temperature °C**	**b_a mV/decade**	**b_c mV/decade**	**E_{corr} mV**	**J_{corr} µA**	**R_p Ω**
M23	20	37.31	24.41	−334	206.10	31.09
	30	33.44	30.29	−332	775.64	8.89
	40	22.89	16.61	−330	894.54	3.93
	50	10.06	12.01	−329	931.25	2.96
M29	20	37.86	21.87	−332	172.55	34.89
	30	34.21	25.06	−336	734.45	9.44
	40	31.89	17.16	−333	884.12	5.55
	50	14.98	11.65	−335	909.08	3.27

Table 8 Electrochemical impedance parameters of maraging specimens in $1MH_2SO_4$ at room temperature

Materials	R_s Ω	CPE mMho	n	R_{ct} Ω
C-250	1	0.993	0.936	12
M23	1	0.956	0.847	30
M29	1.2	1.22	0.762	32.2

ESR (M23 and M29 grade) steels is much less than the C250 steel produced by vacuum melting. Due to lower percent of retained austenite in ESR steels, their corrosion resistance is higher than the C250 steel.

It is evident from the Nyquist plots that the impedance response of C-250 specimens showed a marked difference when compared with ESR steels. The smallest capacitive loop in high frequency range is noticed in C-250 steel as shown in Fig. 9 after 10 min immersion, which reveals the highest corrosion rate for C-250 steel. The EIS parameters such as R_{ct}, R_s and CPE_{dl} for all maraging steels are listed in Table 8 indicating that the values of R_{ct} are less for C250 than ESR steel, i.e., corrosion resistance properties of ESR steel are higher.

4. Conclusions

The electrochemical behavior of ESR maraging steel was investigated at different immersion time and solution temperature in 1 M H_2SO_4 solution using LPP and EIS techniques. These two grades (M23 and M29) of maraging steel were produced through ESR method, and their corrosion resistance behavior has been compared with the conventional maraging steel (C250). The result show that the microstructure of the investigated ESR steels composed of uniform and well-distributed martensite accompanied with little amount of retained austenite in comparison with C250 steel. This could be attributed to the effect of high cooling rate during solidification of produced ingot. From polarization data, it is found that the E_{corr} (versus Ag/AgCl) values shifted toward more anodic (positive) region and J_{corr} values increase due to the dissolution of steel in aggressive sulfuric acid solution. It is also seen that with an increase in the solution temperature, the corrosion resistance of the steels decreases. The corrosion resistance of both cobalt-free maraging ESR steels is higher than that of C250 maraging steel and this may be attributed to electroslag steels characterized by lower amount of retained austenite in microstructure and chemical segregation than the conventional maraging steels.

Acknowledgments

The author extends his appreciation to the Center of Excellence for Research in Engineering Materials (CEREM) of Advanced Manufacturing Institute, King Saud University, Riyadh, Saudi Arabia for funding the work. The steel samples used in this study have been produced and refined at the pilot plant of Steel and Ferroalloys Department, Central Metallurgical Research and Development Institute "CMRDI," Egypt.

References

1. J. Razek, I.E. Klein, and J. Yahalom, Structure and Corrosion Resistance of Oxides Grown on Maraging Steel in Steam at Elevated Temperatures, *Appl. Surf. Sci.*, 1997, **108**, p 159–167
2. Y. Ohue and K. Matsumoto, Sliding-Rolling Contact Fatigue and Wear of Maraging Steel Roller with Ion-Nitriding and Fine Particle Shot-Peening', *Wear*, 2007, **263**, p 782–789
3. W. Wang, W. Yan, Q. Duan, Y. Shan, Z. Zhang, and K. Yang, Study on Fatigue Property of a New 2.8 GPa Grade Maraging Steel, *Mater. Sci. Eng. A*, 2010, **527**, p 3057–3063
4. T. Poornima, J. Nayak, and A.N. Shetty, Corrosion of Aged and Annealed 18 Ni 250 Grade Maraging Steel in Phosphoric Acid Medium, *Int. J. Electrochem. Sci.*, 2010, **5**, p 56–71
5. R.F. Decker and S. Floreen, Intern. Symp. on Maraging Steels Recent Development and Applications, vol. 1 (Pheonix, Arizona, 1998), p. 1–88
6. K. Stiller, F. Danoix, and A. Bostel, Investigation of Precipitation in a New Maraging Stainless Steel, *Appl. Surf. Sci.*, 1996, **94**, p 326–333
7. D. Klobcar, J. Tusek, B. Taljat, L. Kosec, and M. Pleterski, Aging of Maraging Steel Welds During Aluminum Alloy Die Casting, *Mater. Sci.*, 2008, **44**, p 515–522
8. O. Dmitrieva et al., Chemical Gradients Across Phase Boundaries Between Martensite and Austenite in Steel Studied by Atom Probe Tomography and Simulation, *Acta Mater.*, 2008, **59**, p 364–374
9. J. Grum and J.M. Slabe, Effect of Laser-Remelting of Surface Cracks on Microstructure and Residual Stresses in 12Ni Maraging Steel, *Appl. Surf. Sci.*, 2006, **252**, p 4486–4492
10. R.F. Decker, J.T. Eash, and A.J. Goldman, 18% Nickel Maraging Steel, *ASM Trans. Quart.*, 1962, **55**, p 58
11. I.V. Pestov, A. Maloletnev, M.D. Ya Peraks, and N.K. Leonova, *Metall. Term. Obrab. Met.*, 1983, **4**, p 38
12. S. Floreen, Cobalt-Free maraging Steels, H. S. Pat. No. 4443, 1984, p 254
13. D.M. Vanderwalker, *In Maraging Steels—Recent Developments and Applications*, TMS-AIME, Warrendale, PA, 1988, p 255–268
14. H. Halfa, A. Fathy, M. Kamal, M. Eissa and K. El-Fawahkry, Enhancement of mechanical properties of developed Ti-containing Co-free low Ni maraging steel by ESR, STEEL GRIPS 8, 2010, No. Product& Quality, p. 278/284
15. H. Halfa and A.M. Reda, Electroslag Remelting of High Technological Steels, *J. Miner. Mater. Charact. Eng.*, 2015, **3**, p 444–457
16. G. Bellanger and J.J. Rameau, Effect of Slightly Acid pH with or Without Chloride in Radioactive Water on the Corrosion of Maraging Steel, *J. Nucl. Mater.*, 1996, **228**, p 24–37
17. G. Bellanger, Effect of Carbonate in Slightly Alkaline Medium on the Corrosion of Maraging Steel, *J. Nucl. Mater.*, 1994, **217**, p 187–193
18. J. Rezek, I.E. Klein, and J. Yhalom, Electrochemical Properties of Protective Coatings on Maraging Steel, *Corros. Sci.*, 1997, **39**, p 385–397
19. T. Poornima, N. Jagannatha, and A.N. Nityananda, Studies on Corrosion of Annealed and Aged 18 Ni 250 Grade Maraging Steel in Sulphuric Acid Medium, Portugal, *Electrochim. Acta*, 2010, **28**, p 173–188
20. H. Ono, K. Morita, and N. Sano. Metallurg. Mat. Trans. **266B** (1995), p 991/96
21. J. H. Papier, A Stainless Maraging Steel Used in Aerospace Application, The Minerals, Metals & Materials Society, Edited by Richard K. Wilson (1988), p. 125–156
22. J.M. Pardal, S.S.M. Tavares, V.F. Terra, M.R. Da Silva, and D.R. Dos Santos, Modeling of Precipitation Hardening During the Aging and Overaging of 18Ni-Co-Mo-Ti Maraging 300 Steel, *J. Alloys Compd.*, 2005, **393**, p 109–113
23. E.J. Mittemeijer, A. van Gent, and P.J. van der Schaaf, Analysis of Transformation Kinetics by Nonisothermal Dilatometry, *Metal. Trans.*, 1986, **17A**, p 1441–1445
24. P.P. Sinha, D. Sivakumar, N.S. Babu, K.T. Tharian, and A. Natarajan, Austenite Reversion in 18 Ni Co-Free Maraging Steel, *Steel Res.*, 1995, **11**, p 490
25. E.-S.M. Sherif, Corrosion Behavior of Duplex Stainless Steel Alloy Cathodically Modified with Minor Ruthenium Additions in Concentrated Sulfuric Acid Solutions, *Int. J. Electron. Sci.*, 2011, **6**, p 2284–2298
26. A.K. Singh, S.K. Shukla, M. Singh, and M.A. Quraishi, Inhibitive Effect of Ceftazidime on Corrosion of Mild Steel in Hydrochloric Acid Solution, *Mater. Chem. Phys.*, 2011, **129**, p 68–76

27. M. El Azhar, B. Mernari, M. Traisnel, F. Bentiss, and M. Lagrenée, Corrosion Inhibition of Mild Steel by the New Class of Inhibitors [2,5-bis(n-Pyridyl)-1,3,4-thiadiazoles] in Acidic Media, *Corros. Sci.*, 2001, **43**, p 2229–2238
28. J.R. Macdonald and W.B. Johnson, *Theory in Impedance Spectroscopy*, Wiley, New York, 1987
29. H. Wang, X. Wang, H. Wang, L. Wang, and A. Liu, DFT Study of New Bipyrazole Derivatives and Their Potential Activity as Corrosion Inhibitors, *J. Mol. Model.*, 2007, **13**, p 147–153
30. L. Larabi, Y. Harek, O. Benali et al., Hydrazide Derivatives as Corrosion Inhibitors for Mildsteel in 1 M HCl, *Prog. Org. Coat.*, 2005, **54**, p 261